



HAL
open science

Genome wide analysis of the transition to pathogenic lifestyles in Magnaporthales fungi

Ning Zhang, Guohong Cai, Dana C. Price, Jo Anne Crouch, Pierre Gladieux, Bradley Hillman, Chang Hyun Khang, Marc-Henri Lebrun, Yong-Hwan Lee, Jing Luo, et al.

► **To cite this version:**

Ning Zhang, Guohong Cai, Dana C. Price, Jo Anne Crouch, Pierre Gladieux, et al.. Genome wide analysis of the transition to pathogenic lifestyles in Magnaporthales fungi. Scientific Reports, 2018, 8, pp.1-13. 10.1038/s41598-018-24301-6 . hal-02621575

HAL Id: hal-02621575

<https://hal.inrae.fr/hal-02621575>

Submitted on 26 May 2020

HAL is a multi-disciplinary open access archive for the deposit and dissemination of scientific research documents, whether they are published or not. The documents may come from teaching and research institutions in France or abroad, or from public or private research centers.

L'archive ouverte pluridisciplinaire **HAL**, est destinée au dépôt et à la diffusion de documents scientifiques de niveau recherche, publiés ou non, émanant des établissements d'enseignement et de recherche français ou étrangers, des laboratoires publics ou privés.



Distributed under a Creative Commons Attribution 4.0 International License

SCIENTIFIC REPORTS



OPEN

Genome wide analysis of the transition to pathogenic lifestyles in Magnaporthales fungi

Ning Zhang^{1,2}, Guohong Cai³, Dana C. Price⁴, Jo Anne Crouch⁵, Pierre Gladieux⁶, Bradley Hillman¹, Chang Hyun Khang⁷, Marc-Henri LeBrun⁸, Yong-Hwan Lee⁹, Jing Luo¹, Huan Qiu¹⁰, Daniel Veltri¹¹, Jennifer H. Wisecaver¹², Jie Zhu⁷ & Debashish Bhattacharya²

The rice blast fungus *Pyricularia oryzae* (syn. *Magnaporthe oryzae*, *Magnaporthe grisea*), a member of the order Magnaporthales in the class Sordariomycetes, is an important plant pathogen and a model species for studying pathogen infection and plant-fungal interaction. In this study, we generated genome sequence data from five additional Magnaporthales fungi including non-pathogenic species, and performed comparative genome analysis of a total of 13 fungal species in the class Sordariomycetes to understand the evolutionary history of the Magnaporthales and of fungal pathogenesis. Our results suggest that the Magnaporthales diverged ca. 31 million years ago from other Sordariomycetes, with the phytopathogenic blast clade diverging ca. 21 million years ago. Little evidence of inter-phylum horizontal gene transfer (HGT) was detected in Magnaporthales. In contrast, many genes underwent positive selection in this order and the majority of these sequences are clade-specific. The blast clade genomes contain more secretome and avirulence effector genes, which likely play key roles in the interaction between *Pyricularia* species and their plant hosts. Finally, analysis of transposable elements (TE) showed differing proportions of TE classes among Magnaporthales genomes, suggesting that species-specific patterns may hold clues to the history of host/environmental adaptation in these fungi.

The order Magnaporthales in the fungal class Sordariomycetes (Ascomycota) contains economically important pathogens of cereals and grasses, such as the rice blast fungus *Pyricularia oryzae* (syn. *Magnaporthe oryzae*, *Magnaporthe grisea*), the take-all pathogen of cereals *Gaeumannomyces graminis*, and the summer patch pathogen of turfgrasses *Magnaportheopsis poae*. Over 200 species of Magnaporthales have been described, of which about 50% are pathogens of domesticated and wild monocotyledons.

The best studied species in Magnaporthales is the rice blast fungus, which was ranked number one on the “Top 10 fungal plant pathogens” list based on scientific and economic importance in a survey of 495 votes from the international plant mycology community¹. Rice blast is the most destructive disease of rice, which serves as a staple food source for about one-half of the world’s population^{2,3}. This pathogen also infects turfgrasses, causing

¹Department of Plant Biology, Rutgers University, New Brunswick, New Jersey, 08901, USA. ²Department of Biochemistry and Microbiology, Rutgers University, New Brunswick, New Jersey, 08901, USA. ³United States Department of Agriculture, Agricultural Research Service; and Department of Botany and Plant Pathology, Purdue University, West Lafayette, Indiana, 47907, USA. ⁴Department of Plant Biology, Center for Vector Biology, Rutgers University, New Brunswick, New Jersey, 08901, USA. ⁵Mycology and Nematology Genetic Diversity and Biology Laboratory, United States Department of Agriculture, Beltsville, Maryland, 20705, USA. ⁶BGPI, Univ Montpellier, INRA, CIRAD, Montpellier SupAgro, F-34398, Montpellier, France. ⁷Department of Plant Biology, University of Georgia, Athens, GA, 30602, USA. ⁸National Institute of Agricultural Research, Avenue Lucien Brétignières, BP 01, 78850, Thiverval-Grignon, France. ⁹Department of Agricultural Biotechnology, Center for Fungal Genetic Resources, Plant Genomics and Breeding Institute, and Research Institute of Agriculture and Life Sciences, Seoul National University, Seoul, 08826, Republic of Korea. ¹⁰Department of Ecology, Evolution and Natural Resources, Rutgers University, New Brunswick, New Jersey, 08901, USA. ¹¹Bioinformatics and Computational Biosciences Branch, Office of Cyber Infrastructure and Computational Biology, National Institute of Allergy and Infectious Diseases, NIH, Rockville, MD, USA. ¹²Department of Biochemistry, Purdue University, West Lafayette, Indiana, USA. Correspondence and requests for materials should be addressed to N.Z. (email: ningz@rutgers.edu) or D.B. (email: d.bhattacharya@rutgers.edu)

gray leaf spot of perennial ryegrass and tall fescue. This multihost pathogen represents a significant threat to agriculture, as exemplified by recent emergence of wheat blast^{4,5}.

In science, the rice blast fungus is a paradigm for understanding pathogen infection and numerous studies have been performed using this model system. The genome of this fungus was sequenced and released over a decade ago, and genome analysis revealed that it possesses a large set of secreted proteins, an expanded family of G-protein coupled receptors, and ~10% of repetitive elements^{6,7}. The genomes of several other phytopathogenic species in the Magnaporthales have thereafter been sequenced⁸. However, the non-pathogen relatives remain neglected. The paucity of studies and the lack of sequence data from non-model species in Magnaporthales results in a poor understanding of the phylogeny and an unstable taxonomy of Magnaporthales species. Furthermore, genome data from non-pathogen lineages are necessary to provide a more robust comparative genomic framework to help place the rice blast fungus in an evolutionary context and to understand the evolution of pathogenesis and other characters of these important organisms.

To this end, we recently sequenced the genomes of five species and generated transcriptomes from 21 species of Magnaporthales, including saprobes and plant pathogens⁹. Phylogenomic analysis based on these and previously published genome data supported the existence of three major clades that correspond to their pathological characters: species in the “wood” clade are saprobes on submerged wood; species in the “blast” clade produce appressoria and infect leaf tissue of host plants; and those in the “root” clade generally produce hyphopodia and infect plant roots.

Here, we used comparative methods to analyze data from 13 fungal species in the class Sordariomycetes, including nine species in the Magnaporthales, two *Colletotrichum* species and two *Fusarium* species. The nine Magnaporthales species include two saprotrophic non-pathogens (*Ophioceras dolichostomum* and *Pseudohalonectria lignicola*) in the wood clade and seven cereal or grass pathogens (*Gaeumannomyces graminis*, *Magnaporthiopsis poae*, *M. incrustans*, *M. rhizophila*, *Nakataea oryzae* [syn. *Magnaporthe salvinii*], *Pyricularia oryzae* and *P. grisea*) in the blast and root clades. The *Colletotrichum* and *Fusarium* species are also pathogens of plants. The over-arching goal of our study was to develop a comprehensive framework for understanding the evolutionary history of the Magnaporthales and of fungal pathogenesis, by comparing genomic data from plant pathogens and their non-pathogenic relatives. Specifically, we focused on the timeline for Magnaporthales diversification, the extent of horizontal gene transfer (HGT) in this lineage, evidence for positive selection in Magnaporthales genes as a result of environmental adaptation, the nature of the secretome and effectors, and the distribution of transposable elements (TEs) in these genomes.

Results and Discussion

Genome sequencing, assembly, and annotation. For the five Magnaporthales species sequenced for this project (i.e., *M. incrustans*, *M. rhizophila*, *N. oryzae*, *O. dolichostomum*, and *P. lignicola*), the raw sequence reads ranged from 10.2 to 29.6 million read pairs per species for genome data, and 16.4 to 32.6 million read pairs per species for transcriptome data (Table S1). The genome assemblies had a scaffold N50 values that ranged from 62 kbp (179 scaffolds, *N. oryzae*) to 252 kbp (52 scaffolds, *M. rhizophila*), and the contig N50 ranged from 30 kbp (344 contigs, *N. oryzae*) to 60 kbp (205 contigs, *M. incrustans*). There were substantial differences in the assembled genome sizes. *Nakataea oryzae* had the smallest genome (34.9 Mbp), whereas *O. dolichostomum* had the largest (43.0 Mbp). The GC-ratios of these genomes ranged from 54–58%. The smallest number of genes (12,077 genes) was predicted in the smallest genome, *N. oryzae*, whereas the largest number of genes (12,933 genes) was predicted in *M. incrustans*, which had a genome size of 39.3 Mbp. In the largest genome (*O. dolichostomum*), 12,519 genes were predicted (Table S2). *Magnaporthiopsis incrustans* had the largest contig N50, perhaps explaining the larger number of genes predicted from this genome.

To assess the gene inventories in the genome assemblies, CEGMA analyses were done to identify 248 low-copy, core eukaryotic genes. Complete copies of 235 (95%) to 237 (96%) genes were found (Table S3). If partial genes were counted, 97% to 98% of the core genes were found in the genomes, suggesting that the assemblies captured most of the genes in the target taxa. The missing genes were not randomly distributed; i.e., eight genes were missing in two or more genomes (KOG0062, KOG0261, KOG0434, KOG0969, KOG1123, KOG1185, KOG2311, KOG3232). Two genes, KOG1185 (thiamine pyrophosphate-requiring enzyme) and KOG2311 (NAD/FAD-utilizing protein possibly involved in translation) were missing in all five genome assemblies, indicating that these genes either do not exist in Magnaporthales or less likely, all reside in difficult-to-assemble DNA regions.

To facilitate dissemination of the Magnaporthales genome and transcriptome data, we set up an FTP site (<ftp://172.21.7.71/pub/Magnaporthales/>) that includes the assembled genomes and transcriptomes of the five species sequenced for this project, transcriptomes from an additional 16 Magnaporthales species⁹, and the genomes and transcriptomes of eight species that were downloaded from public databases and used in our work. Genome assemblies, annotations, and associated raw sequence reads from this study were submitted to GenBank (BioProject #: PRJNA438993). Using the genome data from the 13 Sordariomycetes species, a total of 14,835 gene families were generated using OrthoFinder that are present in at least two different species. Using a phylogenomic approach, we generated phylogenetic trees for all orthologous gene families and singleton genes. The orthologous gene families and the phylogenetic trees (with ≥ 5 sequences) are available for download from the FTP site and were used for downstream analysis.

Estimating a timeframe for Magnaporthales diversification. We generated a Bayesian maximum credibility tree with mean node age inferred using BEAST, based on 1000 randomly selected single copy orthologs. This phylogeny is shown in Fig. 1. The six replicate MCMCs converged on all parameters, posteriors, and likelihood estimates. The effective sample size values were all >800, and the topology of the tree was identical to the topology of the maximum likelihood tree inferred from the concatenation of the 1000 randomly selected orthologs using RAXML v.8.2.4¹⁰ (not shown). Only results of the run with the highest posterior probability are

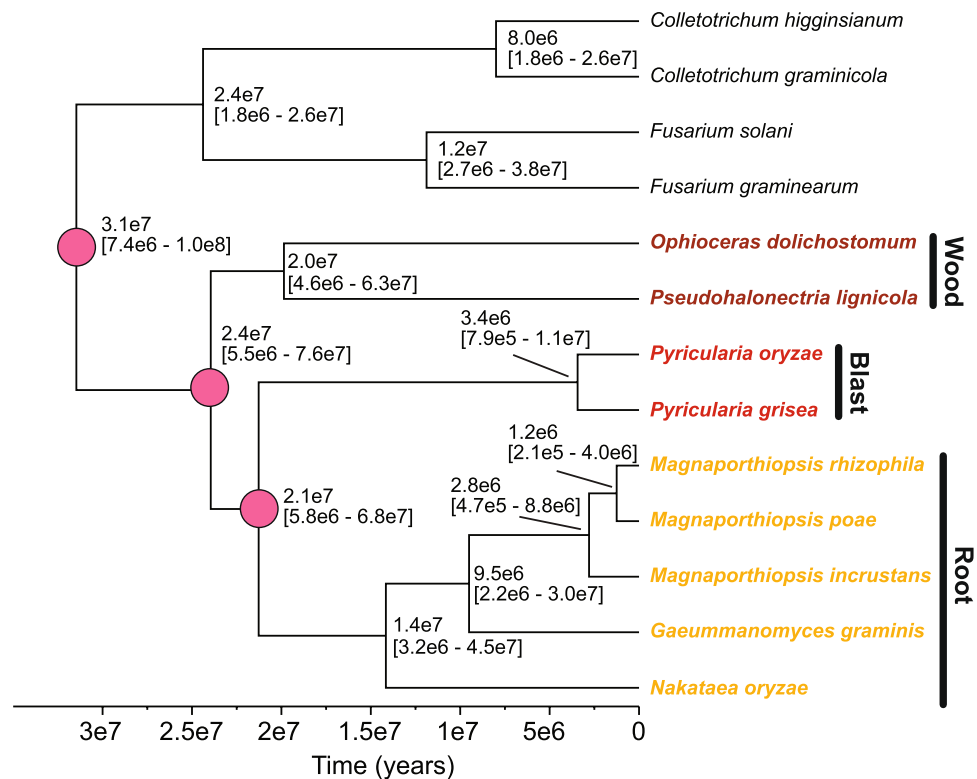


Figure 1. Rooted maximum credibility tree constructed from 1000 single copy orthologous proteins using BEAST. The bootstrap support values were 100 on all branches. Node labels show mean node ages, and 95% highest posterior density intervals. The three clades of Magnaporthales are indicated as are their split dates (with pink filled circles).

presented. All nodes had 100% Bayesian posterior support. The estimates of divergence time indicate that the Magnaporthales diverged ca. 31 million years ago (95% highest posterior density interval [95%HPD]: 7.3e6–10e8) from the group formed by *Colletotrichum* spp. and *Fusarium* spp. (Fig. 1). The split between the wood and blast/root clade occurred about 24 million years ago with the blast clade splitting off about 21 million years ago.

It should be noted, that divergence times estimated from molecular clock analyses largely depend on the values used to define the prior distribution on the substitution rate. In our analysis, the minimum, maximum, and average values of the prior distribution on the substitution rate were defined based on previous estimates of fungal nucleotide substitution rates obtained using different calibration time points (protein clock-based estimate of fungi-animal divergence¹¹, protein clock-based estimate of fungi-plant-animal divergence¹², and ascomycete fossils)¹³. These bounds include the estimate of the substitution rate in *P. oryzae* inferred from a tip-calibrated genome genealogy¹⁴. The minimum and maximum values were also within the range of substitution rates in unicellular eukaryotes¹⁵. Because we used plausible substitution rates and relied on a molecular clock framework that accounted for rate variation along sequences and among lineages, we are confident that our divergence time estimates represent a reasonable approximation for the timeframe of Magnaporthales diversification.

Extent of horizontal gene transfer in Magnaporthales. To assess if HGT may have played a role in the origin of genetic innovations in the studied 13 species of Sordariomycetes, we calculated the Alien Index (AI)^{16,17} for all protein coding genes in each genome. Briefly, for each gene, we compared the strength of its best sequence match in eukaryotes (not including other Sordariomycetes) to its best match in prokaryotes (see Methods). This procedure resulted in a preliminary gene set (516 in total, 0.39%) with significantly stronger hits to prokaryotes than eukaryotes ($AI \geq 0.05$). Depending on the species, the number of genes ranged from 0.24% (in *P. lignicola*) to 0.55% (in *F. solani*). These percentages are similar to those reported in an earlier analysis of bacterium-derived genes in fungi¹⁸. We also examined the corresponding phylogenetic trees generated from our conservative phylogenomic approach described above. A total of 195 cases with conflicting phylogenies (mostly representing more ancient gene transfers earlier than Sordariomycetes ancestor) were filtered out. The remaining 321 cases have trees that are either supportive or inconclusive (regardless of branch support), making them candidates for further investigation (Table S4).

We then focused on HGTs that are specific to the Magnaporthales. A total of five bacterium-derived HGTs were identified that were supported by both the AI-based and phylogenomic methods (Figs 2, S1). These include a gene encoding fumarylacetoacetate hydrolase (FAH, Fig. 2A) that is present in all three Magnaporthales major lineages [wood, blast, and root (Luo *et al.*⁹)]. This gene was most likely transferred into the Magnaporthales common ancestor. FAH participates in amino acid (tyrosine) catabolism hydrolyzing fumarylacetoacetate into

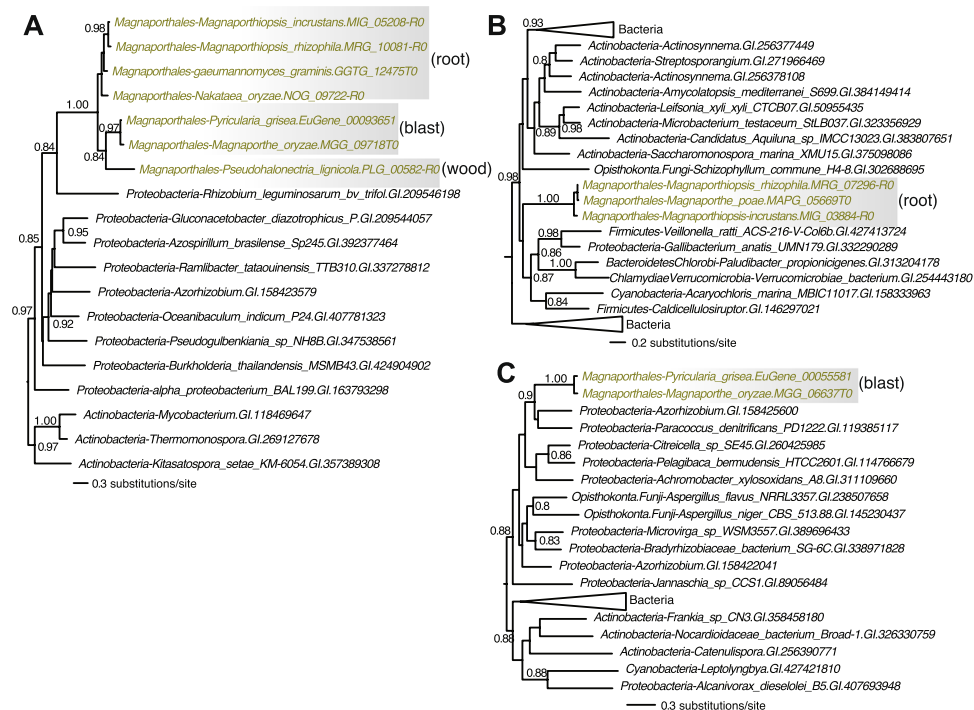


Figure 2. Bacterial-derived HGTs in Magnaporthales. **(A)** Phylogenetic tree of a fumarylacetoacetate hydrolase. **(B)** Phylogenetic tree of a N-acetyltransferase family protein. **(C)** Phylogenetic tree of a N-acetyltransferase family protein. Statistical support (>0.8) is indicated for each branch. Magnaporthales are shown in brown text and prokaryotes in black text. The major clades impacted by HGT (i.e., wood, blast, root) are shown.

fumarate and acetoacetate. We also found the transfer of a gene encoding N-acetyltransferase family (pfam00583) protein into the Magnaporthales root clade (Fig. 2B). Interestingly, another bacterial gene of the same family was transferred independently into the Magnaporthales blast clade (Fig. 2C). Although these two transferred proteins share limited sequence identity (<30%), it is likely that a similar function was independently acquired in these two instances. The remaining two HGTs represent an antibiotic biosynthesis monooxygenase and a hypothetical protein (Fig. S1). Taken together, the small number of HGTs found that are specific to Magnaporthales is consistent with the overall paucity of cross-phylum gene transfers in this lineage¹⁹. Given our focus on a conservative HGT dataset and extensive intra-phylum gene exchanges that may compromise HGT detection¹⁹, these HGTs likely represent a subset of genes that were transferred into Magnaporthales. The existence of clear evidence of bacterium-derived genes suggests that HGT might have played an important role in Magnaporthales evolution and function.

Branch-site selection tests. Beyond HGT, genetic innovation can also result from positive selection acting on fungal genes in response to environmental constraints or life cycle evolution. To address this issue, we did enrichment tests on the genome data (see Methods). This analysis identified 447, 611, and 610 ortholog groups (OGs) that show evidence of positive selection (FDR ≤ 0.01) in the wood, blast, and root infecting fungal clades⁹ (Table S5). Blast2GO enrichment analyses highlighted 54, 42, and 25 over-represented “most specific” gene ontology (GO) terms in each group, respectively (Tables S6, S7). Examination of this list allowed us to identify shared and lineage-specific GO terms and OGs that shed light on particular genes and gene families and molecular mechanisms responsible for phenotypic and phylogenetic diversification of the Magnaporthales fungal clades. Only 81 of the 1,211 total OGs showing evidence of positive selection were shared in all three clades tested; the majority are specific to individual clades (Fig. 3). The root and blast fungal clades shared the highest number of OGs, likely owing to their common ancestry⁹. Particular attention was given to enriched GO terms from within individual wood, blast, or root clades comprised predominantly of OGs not present in the remaining two groups (Tables S6, S7), because these would represent clade- or lineage-specific targets of selection. We focused on these terms for the remaining discussion below.

Gene ontologies enriched in the blast clade include those involved in DNA repair (GO:0003684 *damaged DNA binding*, GO:0019985 *translesion synthesis*, GO:0035267 *NuA4 histone acetyltransferase complex*), signaling and response to stimulus (GO:0009607 *response to biotic stimulus*, GO:0046578 *regulation of Ras protein signal transduction*), malic enzyme activity (GO:0006108 *malate metabolic process*, GO:0016615 *malate dehydrogenase activity*), glutamate synthase/dehydrogenase activity (GO:0009064 *glutamine family amino acid metabolic process*, GO:0016639 *oxidoreductase activity, acting on the CH-NH2 group of donors, NAD or NADP as acceptor*), synthesis and catabolism of small molecules (GO:0046165 *alcohol biosynthetic process*, GO:0044282 *small molecule catabolic process*) along with genes involved in septation during cytokinesis²⁰ (GO:0005826 *actomyosin contractile ring*).

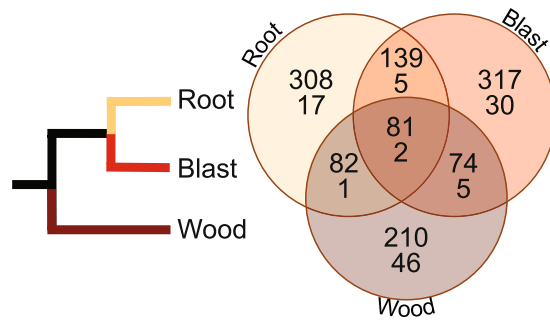


Figure 3. Schematic phylogeny (left image) of the three major Magnaporthales clades proposed by Luo *et al.*⁹ The right image is a Venn diagram showing shared and unique ortholog groups (OGs, top number) and gene ontology terms (GO terms, bottom number) that show evidence of positive selection among the three lineages.

The root infecting fungal branch was enriched for ontologies primarily associated with peptidases (GO:0004222 *metalloendopeptidase activity*, GO:0004252 *serine-type endopeptidase activity*), small molecule metabolic processes (GO:0009132 *nucleoside diphosphate metabolic process*, GO:0015940 *pantothenate biosynthetic process*), transferases (GO:0016409 *palmitoyltransferase activity*, GO:0016757 *transferase activity, transferring glycosyl groups*, GO:0070566 *adenylyl transferase activity*), isomerases (GO:0016853 *isomerase activity*) as well as gene families involving the function and morphology of the fungal-type vacuole (GO:0000324 *fungal-type vacuole*), a lytic membrane-bound compartment that functions in degradation and also stores small molecules²¹.

The more diverged and niche-adapted saprotrophic wood-inhabiting fungi showed evidence of positive selection on the largest number of ontologies, including those involved in chromatin and chromosome modification (GO:0000083 *regulation of transcription involved in G1/S transition of mitotic cell cycle*, GO:0000414 *regulation of histone H3-K36 methylation*, GO:0035327 *transcriptionally active chromatin*, GO:0016233 *telomere capping*, GO:0000118 *histone deacetylase complex*, GO:0051568 *histone H3-K4 methylation*), transcription and RNA processing (GO:0098781 *ncRNA transcription*, GO:0032545 *CURI complex*, GO:0006409 *tRNA export from nucleus*), the (endo)membrane system (GO:0005643 *nuclear pore*, GO:0017056 *structural constituent of nuclear pore*, GO:0032541 *cortical endoplasmic reticulum*, GO:0090158 *endoplasmic reticulum membrane organization*, GO:0060304 *regulation of phosphatidylinositol dephosphorylation* [phosphatidylinositol is a key membrane constituent]), the spliceosomal complex (GO:0000244 *spliceosomal tri-snRNP complex assembly*, GO:0005682 *U5 snRNP*), and organelle and cytoskeletal organization (GO:0034631 *microtubule anchoring at spindle pole body*, GO:0036257 *multivesicular body organization*).

We also examined the seven over-represented GO terms shared between the root and blast pathogenic fungal clades (Table S6), because these may comprise common gene families that elucidate pathogen adaptation. Of the seven terms, six (GO:0030422 *production of siRNA involved in RNA interference*, GO:0031048 *chromatin silencing by small RNA*, GO:0031332 *RNAi effector complex*, GO:0051570 *regulation of histone H3-K9 methylation*, GO:0031618 *nuclear pericentric heterochromatin*, GO:0033562 *co-transcriptional gene silencing by RNA interference machinery*) contain a common group of enzymes (Argonaute-binding 1, dicer 1, piwi domain-containing) that implicate the RNA interference pathway, whereas the final term (GO:0031573 *intra-S DNA damage checkpoint*) describes a pathway that slows DNA synthesis in response to DNA damage²². Both RNAi and small RNAs have recently been shown to facilitate infection of plant hosts by fungal pathogens²³, and components of the DNA damage checkpoint also appear to function in the switch from unicellular growth to the hyphal stage (the infectious stage in pathogenic fungi) in *Schizosaccharomyces* species²⁴. These particular GO terms may therefore highlight drivers of differentiation and adaptation in fungal pathogens. We analyzed the 139 OGs shared between the root and blast clades that show evidence of selection and extracted the most abundant GO term from the annotations (irrespective of statistical representation). This term was GO:0016021 *cellular component of membrane* (28 occurrences), indicating membrane-anchored components are widespread in this subset of genes.

Secretome and effectors in Magnaporthales. Moving from the molecular evolution of pathogenic Magnaporthales genomes, we next focused on the secretome of this clade and encoded effectors. The results of this analysis for the sizes of the secretome and small secreted proteins (SSPs), and species-specific SSPs in Magnaporthales species (SSSPs) are listed in Table 1 and the identifiers are provided in Table S8. The clade-specific secretomes and SSPs were also identified (see Table 2, identifiers in Table S9). The two species in the blast pathogen clade, *P. grisea* and *P. oryzae* had the highest number of secretome, SSPs, and SSSPs when compared to the other Magnaporthales species. The blast pathogens also had remarkably more clade-specific secretomes (454) and SSPs (385) than the root pathogen clade (15 and 12 respectively) and the wood non-pathogen clade (55 and 31).

Our analysis of effectors revealed both clade-specific effectors and ones that are conserved across multiple clades with a varying number of homologs (Fig. 4). The clade-specific effectors include eight avirulence genes that are exclusively present in various strains of *P. oryzae* and *P. grisea*, belonging to the blast clade. Increasing evidence suggests that avirulence genes can also play roles in infection of susceptible hosts^{25,26}. For example, an avirulence gene *AvrPiz-t* encodes a secreted protein that enters the host cytoplasm, where it interacts with the rice RING E3 ubiquitin ligase APIP6 to suppress PAMP-triggered immunity (PTI). Given the blast clade-specific occurrence of these avirulence genes, their known and presumed roles are likely to be specific to the interactions between *Pyricularia* species and their hosts.

Species	Secretome	SSPs	SSSPs
<i>G. graminis</i>	1,204	545	91
<i>P. grisea</i>	1,369	743	143
<i>P. oryzae</i>	1,426	772	221
<i>M. poae</i>	1,076	565	58
<i>M. incrustans</i>	1,203	528	54
<i>M. rhizophila</i>	1,136	490	29
<i>N. oryzae</i>	1,075	460	81
<i>O. dolichostomum</i>	1,022	432	110
<i>P. lignicola</i>	1,038	410	93

Table 1. Predicted secretome size in different Magnaporthales species.

Clade	Secretome	SSPs
Blast pathogen clade	454	385
<i>P. oryzae</i>	227	191
<i>P. grisea</i>	227	194
Root pathogen clade	15	12
<i>M. poae</i>	4	4
<i>M. incrustans</i>	4	4
<i>M. rhizophila</i>	3	2
<i>N. oryzae</i>	4	2
Wood (non-pathogen) clade	55	31
<i>O. dolichostomum</i>	29	15
<i>P. lignicola</i>	26	16

Table 2. Clade-specific secretomes and small secreted proteins (SSPs).

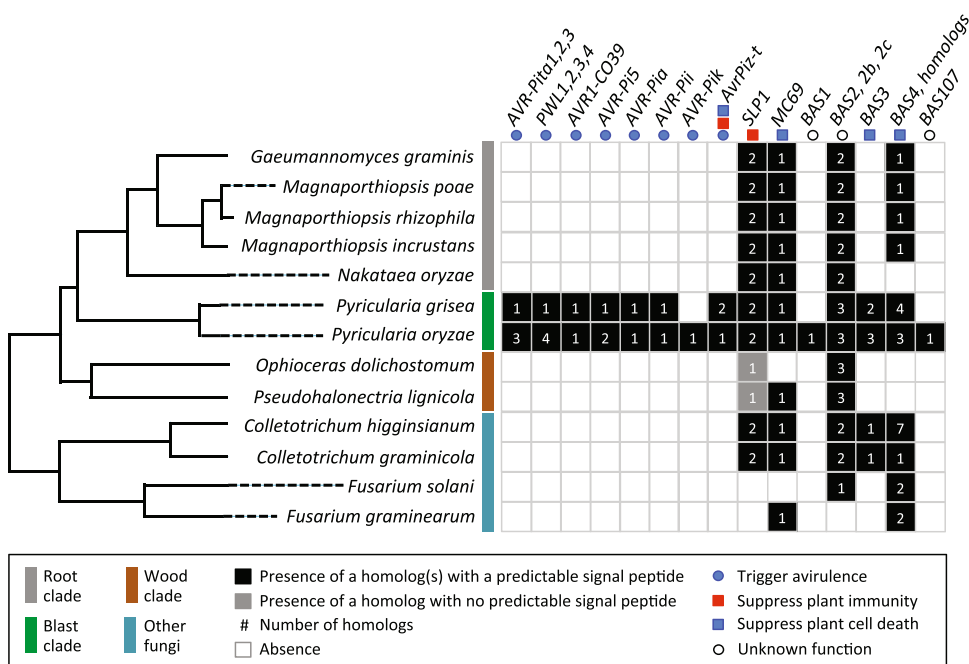


Figure 4. Distribution of different effectors in the Magnaporthales showing the existence of both clade-specific and more widely conserved genes.

Another host PTI suppressor, Slp1, has been characterized in *P. oryzae*. Slp1 is a secreted LysM protein that suppresses host PTI by scavenging PAMP molecules such as chitin in the apoplast, thus being required for *P. oryzae* virulence²⁷. LysM proteins are highly conserved across fungi, and in particular, Slp1 shows strong similarity to the Ecp6 chitin binding protein found in *Cladosporium fulvum*²⁷. Not surprisingly, we found that Slp1 homologs were present in all Magnaporthales and *Colletotrichum* species (Fig. 4). Interestingly, the wood clade fungi carry

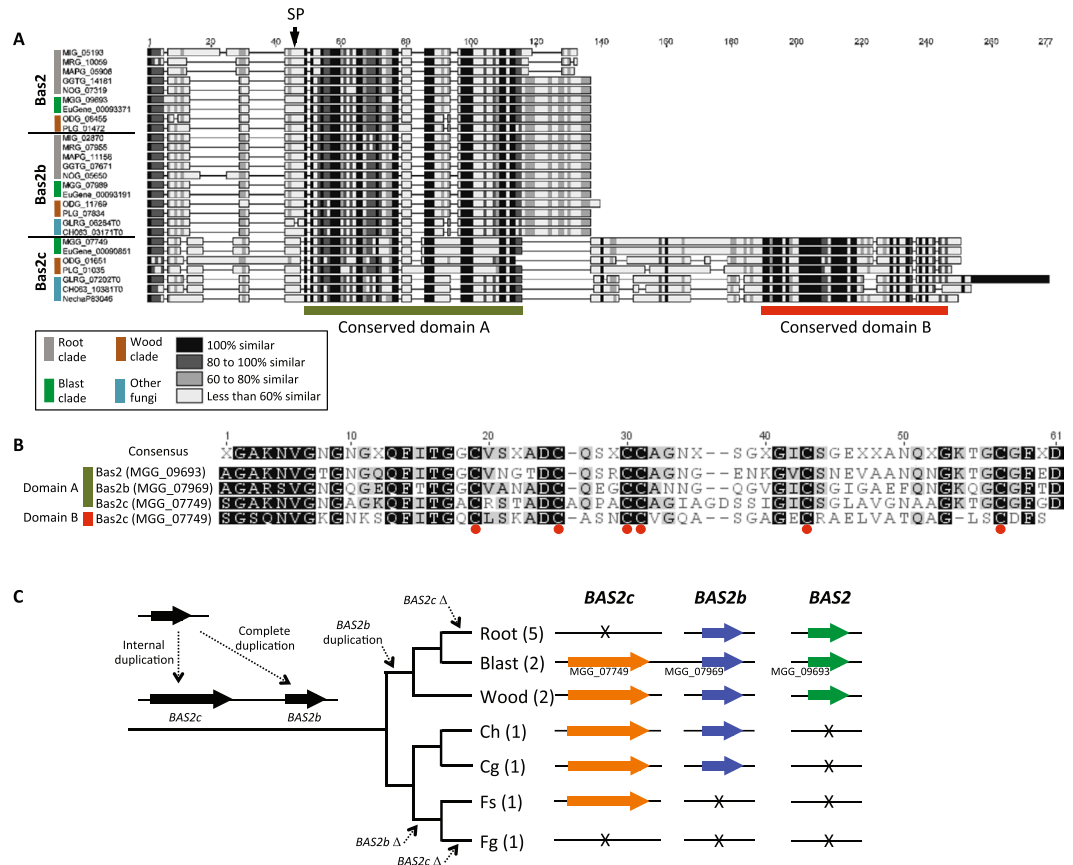


Figure 5. Analysis of Bas proteins in the Magnaporthales. (A) Domain structure between gene family members. (B) Alignment showing conserved residues. (C) Phylogenetic distribution of Bas proteins and history of gene/domain duplication among the three major Magnaporthales clades.

one Slp1 homolog that lacks a predictable signal peptide, suggesting that this protein may have a divergent function than other secreted Slp1 homologs. Three effectors suppress plant cell death²⁸, and are required for *P. oryzae* to establish biotrophy at the early stage of rice infection. These effectors include MC69 (MGG_02848), which is essential for full virulence of *P. oryzae* and is conserved in many plant pathogenic fungi²⁹, and two Bas proteins Bas3 (MGG_11610) and Bas4 homologue (MGG_02154) (Fig. 4).

BAS2 (MGG09693) belongs to a multigene family with two other members³⁰, named here as *BAS2b* (MGG07969), and *BAS2c* (MGG07749). We found that all sequenced genomes included in this study, with the exception of *F. graminearum*, encode at least one member of the family (Fig. 4; Tables S8, S9). The wide occurrence of the *BAS2* family suggests its role in fungal adaptation to diverse hosts and environments. To gain insights into the role of these effectors in fungal adaptation, we reconstructed the evolution of the *BAS2* family by analyzing the presence/absence polymorphism and sequence similarity of the family members. Our analysis revealed that *BAS2* and its orthologs were present only in Magnaporthales, suggesting they were derived from Magnaporthales-specific gene duplication. The presence of the orthologs of *BAS2b* and *BAS2c* in *Colletotrichum* species and their absence in some lineages support their ancestral presence and subsequent loss in respective lineages. In the sequenced genome of *P. oryzae* strain 70–15, *BAS2* is located on chromosome IV, whereas *BAS2b* and *BAS2c* are located ~800 kb apart on chromosome III. Chromosomal locations of *BAS2* homologs found in other sequenced genomes remain undetermined due to gaps in genome assemblies. Interestingly, *BAS2c* and its orthologs encode larger-secreted proteins, ranging from 173 to 204 residues, than those of *BAS2* (86–101 residues) or *BAS2b* (99–108 residues). A dot plot analysis and sequence comparison revealed that the *Bas2c* protein contained two domains that share high sequence similarity with each other and also six conserved Cys residues in each domain (Fig. 5; Tables S8, S9). These data suggest that *BAS2c* resulted from an internal gene duplication, which likely led to the gain of a new function, potentially providing a beneficial adaptation³¹. Consistent with this idea, targeted gene replacement of *BAS2* does not result in pathogenicity phenotypes³⁰, possibly due to functional redundancy with its duplicate, *BAS2b*. We propose that the *BAS2* gene family has undergone both internal and complete gene duplications to generate functionally divergent family members as well as multiple losses during fungal adaptation to diverse habitats.

Analysis of transposable elements. Each of the nine genomes, plus that of *Falciophora oryzae* (syn. *Harpophora oryzae*), were individually checked for TEs using the REPET vr. 2.5 pipeline. The combined length of all TE matches identified by REPET as a percentage of genome size is shown in Fig. S2A. These results ranged

from 0.64% (253,718 bp) for *M. poae* to 15.35% (7,795,925 bp) for *F. oryzae*. We note the proportion of TEs shown is approximately the same as the numbers previously reported by Xu *et al.*³² for *F. oryzae* (+0.4%), *P. oryzae* (+1.7%), *M. poae* (−0.01%) and *G. graminis* (−0.3%) (Fig. S2A). These small differences in the overall proportion of TEs likely stem from Xu *et al.* using a different program, RepeatModeler³³, for their TE prediction protocol. Class I TEs (retrotransposons) were found to be more abundant than Class II TEs (DNA transposons) across all genomes. The ratio of Class I to Class II TE percentages shown ranges from 2:1 for *M. oryzae* to almost 20:1 for *M. rhizophila* (Fig. S2A).

The relative abundance of TEs as a percentage of genome size, when grouped by TE order is shown in Fig. S2B. Long terminal repeat (LTR) TEs were found to be the most abundant Class I order for all surveyed genomes. Consistent with previous reports⁶, the LTR retrotransposons, were the most abundant order of TEs in the genome of *M. oryzae* (3.3% of all TEs), but our analysis showed that members of the DIRS family were found in nearly as high abundance (3.2% of all TEs). Amongst Class II orders, terminal inverted repeats (TIRs) were the most abundant for all genomes with the exception of *M. incrustans*, which encoded more Helitrons. At the superfamily level, Gypsy was generally the most abundant TE, followed by Copia. Analysis of novel TEs and evidence of repeat-induced point mutation (RIP) are described in the Supplementary Text.

TEs have been shown as important drivers of genome evolution in the several species of Magnaporthales^{6,32,34–36}. For example, in *F. oryzae* TEs have played a major role in the lifestyle transition from parasite to beneficial endophyte during rice root infections by causing species-specific gene expansions^{32,37}. The species-specific nature of these TE expansions in the Magnaporthales can be observed in Fig. S2A, where the percentage of the genome occupied by TEs varies greatly. Even amongst *F. oryzae*, *G. graminis*, and *M. poae*, which all infect rice roots and share high levels of macrosyteny³², both the lowest and highest TE percentages in Fig. S2A are seen with *M. poae* and *F. oryzae* (a difference of 14.7%). Whereas environmental differences amongst all taxa likely explains much of the variability in the number of TEs present, the role of RIP in limiting TE expansion is another factor that is relevant in the genome of *M. oryzae*⁶. RIP was found present in almost 80% of the TE superfamilies assessed in Fig. S3 and in at least one family for all genomes considered except for *O. dolichostomum* and *M. rhizophila*. One possibility for RIPs not being identified in the latter two species is the large number of unclassified LTR, LINE, and TIR sequences found using REPET. Collectively, these unknown TEs account for 1.3% and 5.8% of the *O. dolichostomum* and *M. rhizophila* genomes, respectively. Accordingly, many of these sequences may belong to TE superfamilies that did not meet the quantity or length requirements used to test for RIP using RIPCAL. Amongst the TEs identified across genomes, Class I members were found to consistently outnumber those in Class II. LTRs and TIRs were generally found to be the most prevalent Class I and Class II TE orders, respectively. Finally, analysis of REPET *de novo* predicted TE families identified many clusters with high similarity to known AVR genes in *M. oryzae*. This lends further support to the importance of TEs in shaping fungal-plant interactions amongst the Magnaporthales.

Conclusions

Our study provides a genome-based perspective on the evolution of Magnaporthales, suggesting that this order diverged from other Sordariomycetes about 31 million years ago with the phytopathogenic blast clade diverging ca. 21 million years ago. We find little evidence of HGT among these taxa, with only a handful of *bona fide* candidates, although intra-phylum gene movement may be much higher but was not the target of our conservative phylogenomic approach. In contrast, many more genes underwent positive selection in Magnaporthales with only 81/1,211 OGs in this category being shared by all three clades. The majority are clade-specific, with the wood clade having the largest number of gene ontologies impacted by positive selection. Analysis of the secretome and effectors showed that the blast clade is most enriched in the latter as avirulence genes. These likely play key roles in the interaction between *Pyricularia* species and their plant hosts. Finally, analysis of TEs showed different proportions of TE classes in the Magnaporthales genomes, suggesting that species-specific patterns may hold clues to the history of host/environmental adaptation in these lineages. We did not include in this manuscript an analysis of biosynthetic pathways of secondary metabolites in Magnaporthales. Nonetheless, we recognize that these gene clusters are of significant interest to mycologists, in particular, the comparison of pathways in pathogenic and non-pathogenic fungi. We hope that the genome data produced here will enable investigation of this and other important topics in the near future. In summary, our comparative analyses point out the divergent histories of fungi in the important Magnaporthales order and provide clues to how these taxa have adapted to their vastly different niches in the past 31 million years.

Methods

Genome sequencing, assembly and annotation. Five species in Magnaporthales, *M. incrustans* (strain M35), *M. rhizophila* (strain M23), *N. oryzae* (strain M69), *O. dolichostomum* (strain CBS114926) and *P. lignicola* (strain M95) were subjected to genome and transcriptome sequencing in this project. For genome sequencing, DNA was extracted from mycelium after 14 days of growth on potato dextrose agar (PDA) at 25 °C using DNeasy Plant Mini Kit (Qiagen, CA). A Nextera DNA library with average insert size approximately 450 bp was constructed for each species following manufacturer's instructions (Illumina). The libraries were sequenced to 2 × 146 bp on GenomeAnalyzer IIX (Illumina). For transcriptome sequencing, strains were grown at 25 °C on four different conditions: PDA under 12/12 hours light-dark cycle, PDA in constant darkness, minimal medium (MM, 10 g sucrose, 1 g Ca(NO₃)₂·4H₂O, 0.2 g KH₂PO₄, 0.25 g MgSO₄·7H₂O, 0.15 g NaCl, and 15 g agar in 1 liter distilled water) under 12/12 hours light-dark cycle, MM in constant darkness. A cellophane membrane was placed on top of the media. After 14 days of incubation, the mycelium was harvested and total RNA extracted from each sample using the Plant RNeasy Mini Kit (Qiagen, CA). A TruSeq mRNA library was constructed for each sample following manufacturer's instructions (Illumina). The libraries were sequenced on MiSeq (Illumina) to 2 × 158 bp.

Adapter sequences were trimmed from sequence reads of genomic DNA using Trimmomatic³⁸. Trimmed reads were corrected using the correction module in SOAPdenovo2 r239 package³⁹ with k-mer size 21. Corrected reads were assembled using SOAPdenovo2. A range of k-mer sizes were tested and optimal k-mer sizes were chosen for individual genomes. Scaffolds and singleton contigs less than 500 bp in length were filtered out from final assemblies. To test the completeness of assembled genomes, CEGMA (Core Eukaryotic Genes Mapping Approach)^{40,41} analysis was used to look for the 248 conserved eukaryotic genes in assembled genomes.

The assembled genomes were annotated using the MAKER2 package⁴² with three gene prediction tools used: AUGUSTUS^{43,44}, SNAP⁴⁵ and the *ab initio* tool GeneMark-ES version 2⁴⁶. AUGUSTUS was trained with *M. oryzae*, and SNAP was initially trained with CEGMA results. MAKER2 was run for four iterations for each genome. Gene models from the previous run were used for re-training in the following run. Adapter-trimmed transcriptome sequences were used to assemble EST sequences with TRINITY⁴⁷ using the assembled genomes as guide. The results were used as EST evidences in MAKER2 runs. Proteome sequences of *G. tritici* strain R3-111a-1, *M. oryzae* strain 70-15_8 and *M. poae* strain ATCC64411, and the manually annotated Swiss-Prot⁴⁸ protein sequences were used as protein evidences. The flanking regions were set to 50 bp to mitigate gene model fusion which could occur in compact fungal genomes. After four iterations, the optimal gene models chosen by MAKER2 from the three gene prediction tools were used for downstream analysis.

Sequence availability. Genome assembly, transcriptome and proteome sequences of eight species were downloaded from public databases. Those of *C. graminicola* strain M1.001, *C. higginsianum* strain IMI 349063, *F. graminearum* strain PH-1, *G. tritici* strain R3-111a-1, *M. oryzae* strain 70-15_8 and *M. poae* strain ATCC64411 were downloaded from Broad Institute (<http://www.broadinstitute.org/ftp/pub/annotation/fungi/>); those for *F. solani* was obtained from ENSEMBL (ftp://ftp.ensemblgenomes.org/pub/fungi/release-30/fasta/fusarium_solani/); and files for *P. grisea* strain BR29 were obtained from INRA (<http://genome.jouy.inra.fr/genom/>).

Construction of orthologous gene families. We collected proteome data from the 13 Sordariomycetes species described above. After removing short sequences (<50 amino acids), a total of 171,033 sequences were used to construct orthologous gene families using OrthoFinder version 0.4⁴⁹ under the default setting (BLASTp e-value cut-off = 1e-5; MCL inflation I = 1.5). A total of 14,835 gene families were generated that are available at our FTP site (<ftp://172.21.7.71/pub/Magnaporthales/>).

Timing of Magnaporthales diversification. Divergence time estimates were based on a subset of 1000 orthologs randomly selected (using python package random) from the full set of 3,060 single copy orthologs. The 3,060 groups were selected by parsing the ortholog groups (OGs) derived above, and keeping only single-copy genes (i.e., had no evidence of duplication) in all 13 taxa. Sequences were aligned using MACSE⁵⁰, with default parameters. MACSE alignments were processed to remove all codons including sites with a gap in at least one of the samples, and then concatenated. Node ages were estimated using a Bayesian molecular clock model implemented in the program BEAST v1.8.0^{51,52}. The analysis used a General Time Reversible model (GTR) with Gamma distribution for modeling site heterogeneity and base frequencies estimated from the data. The clock model was a random local clock, and the coalescent tree prior assumed an unknown constant population size back through time. We specified the normal prior distributions on substitution rates. We used the minimum and maximum values of exonic substitution rates estimated by Kasuga *et al.*⁵³ using fossil-calibrated phylogenies as the lower and upper bounds (0.13e-9 and 1.759e-8 substitutions/site/year, respectively). The initial value and the mean were set at 8.86e-9 substitutions/site/year [(0.13e-9 + 1.759e-8)/2], and the standard deviation was 1e-8. We edited the XML file generated by BEAUti v.1.8.2. to estimate the age of all nodes in the tree. We used UPGMA tree as the starting tree and ran six independent MCMC of 7.5e7 steps to ensure convergence, logging parameters and trees every 7500 steps. The program Tracer v1.5⁵² was used to evaluate all chains, determine appropriate burn-in length (10% of sampled trees), and obtain the effective sample sizes for all parameters. Mean node age and 95% highest posterior density were mapped on the maximum clade credibility tree.

Screen for HGT candidates. For each Sordariomycetes genome, all predicted proteins were queried against NCBI's non-redundant protein database (November 10, 2015) using ublast with database seq masking enabled, dbacc parameter of 100, accel parameter of 1, and e-value cutoff of 0.001 (<http://drive5.com/usearch>)⁵⁴. A modified alien index approach¹⁶ was used to screen each genome for genes with significantly better ublast hits to prokaryotes than eukaryotes and thus identify trans-domain HGT candidates. The AI score for this analysis is given by the formula:

$$AI = \left(\frac{bbhO}{maxB} - \frac{bbhE}{maxB} \right),$$

where *bbhO* is the bitscore of the best blast hit to a species outside of the eukaryotic lineage, *bbhE* is the bitscore of the best blast hit to a eukaryote, and *maxB* is the maximum bitscore possible for the query sequence (i.e., the bitscore of the query aligned to itself). To identify horizontally transferred genes shared between multiple species of Sordariomycetes (e.g., HGT that occurred in a common ancestor), all hits to Sordariomycetes were skipped and did not contribute to *bbhE*. *AI* can range from 1 to -1, and *AI* > 0 if the gene has a better blast hit to a species outside of the eukaryotic lineage and is suggestive of either HGT or contamination. Contamination was suspected in cases when the majority of genes on an assembly contig had an *AI* ≥ 0; in contrast, HGT was inferred when the transferred gene was located within a well assembled contig, and the majority of genes on that contig had an *AI* < 0⁵⁵. The perl script for calculating AI scores is freely available from the figshare repository, <https://doi.org/10.6084/m9.figshare.1593040>.

Phylogenomic analysis. To understand the evolutionary history of each Sordariomycetes gene, we carried out phylogenomic analysis in a similar way to our previous study¹⁹. Briefly, a local database was established containing Pezizomycotina sequences from NCBI RefSeq database (version 69) and the sequences for the remaining species from RefSeq database (version 55)¹⁹. For each Sordariomycetes orthologous gene family and singlet, we used the corresponding protein sequence(s) as query to search the above-mentioned local database using BLASTp (e-value cut-off = $1e-5$). For each singlet query, the top 1,200 significant hits (with query-hit identity $\geq 30\%$) were recorded followed by selection of representative sequences in order. Up to 10 sequences were sampled from each phylum. The sequence sampling ceased when a total of 80 sequences were selected or the entire list of significant hits was read through. For the gene families containing two or more members, the quota for sequence sampling was divided among members and the sampled sequences were pooled. When the sampled unique sequences were less than 80, further rounds of sequence sampling were carried out until more than 80 unique sequences were sampled. The retrieved sequences were combined with query sequences and were then aligned using MUSCLE version 3.8.31⁵⁶ under default settings followed by trimming using TrimAl version 1.2⁵⁷ in an automated mode (–automated1). We removed columns with $>50\%$ gaps and the resulting alignments were then used to build phylogenetic trees using FastTree⁵⁸ under the WAG + CAT model with four rounds of minimum-evolution SPR moves (–spr 4) and exhaustive ML nearest-neighbor interchanges (–mlacc 2 –slowini). Branch supports were calculated using the Shimodaira-Hasegawa method⁵⁹.

Branch-site selection tests. The corresponding protein sequences that composed the OG were aligned with MAFFT v7⁶⁰ and a codon alignment for each OG was then created with TranslatorX⁶¹ using the nucleotide CDS sequence and aligned protein data as a guide. MaxAlign v1.1⁶² was used in codon mode to remove poorly aligned sites and sequences. Any taxa removed from the OG by MaxAlign were then removed from the phylogenetic tree (above) using PareTree (<http://emmahodcroft.com/PareTree.html>). The branch-site selection test implemented in codeml (part of the PAML package v.4.8a)⁶³ was then used to test for positive selection on three branches of the phylogeny leading to the “wood”, “blast” and “root” fungi (see above)⁹. If all taxa within a particular clade (i.e. both *Pseudohalonestria lignicola* and *Ophioceras dolichostomum* or “wood” saprophytic fungi)⁹ were removed by PareTree, the OG was ignored for that particular test. The log-likelihoods generated by codeml under a null hypothesis of neutral evolution (omega fixed at 1) and the alternative (ML estimate of omega) were compared using a likelihood ratio test to a chi-square distribution (df = 1) and false discovery rate (FDR) tests were performed in R using the Bioconductor package. Ortholog groups with a corresponding test statistic (FDR ≤ 0.01) were retained. Gene Ontology terms were assigned to each gene in each OG using Blast2GO⁶⁴, and annotated further against the NCBI nr database using BLASTp. A Fisher’s exact test was conducted in Blast2GO to find enriched (or over-represented) GO terms ($p \leq 0.05$) within the set of OGs found to be under positive selection as compared to a reference set consisting of all 3,060 OGs. GO terms were condensed to “most specific terms”, i.e. less descriptive parent terms in the hierarchy were removed and only the most-descriptive child terms were retained. If an OG was excluded from the “wood”, “blast” or “root” analysis based on MaxAlign criteria, it was also removed from the reference.

Whole-proteome MCL clustering analysis. The whole-proteome clustering analysis for 9 Magnaporthales spp. and 4 closely related species was performed using the MCL algorithm (<http://micans.org/mcl/>)⁶⁵. The parameters used for clustering were the same as for orthologous gene group prediction (BLASTp: $E = 1e-5$, MCL clustering inflation = 1.5).

Secretome analysis. The secretome of the nine Magnaporthales species were predicted using the pipeline described in Kim *et al.*⁶⁶ and the number of small secreted proteins (SSPs, <300 aa) were counted. The pipeline strictly excludes membrane-bound secreted proteins (both transmembrane helix containing and GPI-anchored proteins); therefore, the predicted secretome sizes are generally smaller than the ones only predicted with signalP Eukaryotes. The number of SSPs were further reduced by comparing to above species-specific clustering data to find the ones with effector-like property, which are referred as SSSPs. Based on the whole protein OrthoFinder clusters and the secretome results, clade-specific secretomes were also identified.

Many plant pathogenic fungi secrete effector proteins that facilitate disease development and modulate plant immunity. However, avirulence effectors trigger defense responses in hosts with cognate R genes and block disease. From various strains of *P. oryzae*, over 200 effector and effector candidate genes have been identified, some of which belong to multigenic families^{28,67}. Of these, we selected 28 well-characterized effector genes and their homologs to survey for their presence in 13 sequenced genomes of nine Magnaporthales species and four closely related fungal pathogens including *Colletotrichum* species and *Fusarium* species.

TE identification. Each of the nine Magnaporthales genomes, plus the genome for *Falciphora oryzae*, were searched for TEs using the REPET vr. 2.5 pipeline³³ according to the authors’ documentation (<https://urgi.versailles.inra.fr/Tools/REPET>). The pipeline begins with the *TEdenovo* script, which uses a series of classifiers to identify a set of *de novo* TEs which are combined to form a database for use with the second *TEannot* script. This latter stage is run twice in order to perform a complete genome-wide annotation using multiple classifiers. A step is also performed which employs tBLASTx and BLASTx from the BLAST + vr. 2.2.31 package⁶⁸ to search Repbase vr. 20.05⁶⁹, a curated data bank of TEs. Both stages were run using default settings and also incorporated the Pfam vr. 27.0⁷⁰ data bank. After identifying TEs throughout the genome, final annotation was exported as a GFF3 file using an option to merge overlapping TE entries. Counts of TE superfamilies were made for each genome using these files according to the Wicker classification scheme⁷¹. According to recommendations by Wicker *et al.*⁷¹, sequences less than 80 bp in length were excluded to avoid misclassification. Other TEs removed included potential host genes and predictions made from tBLASTx and BLASTx with less than 70% sequence identity reported.

As some genomes had many hits classified by family and order, but listed as “unknown” for superfamily (e.g. *DTX*, an unknown Class II terminal inverted repeat), we ran an additional tBLASTx search (e-value: 0.01, percent query coverage per hsp: $\geq 70\%$, minimum percent identity of hits: $\geq 70\%$) against Repbase for these sequences. If a top hit matching the above search criteria had the same family and order as the original REPET prediction, we reassigned the superfamily based on the matching Repbase entry. Additional details about the REPET pipeline can be found in Flutre *et al.*³³.

Cross-genome comparison of REPET *de Novo* TEs. Similarity across genomes for TEs predicted by the REPET *TEdenovo* pipeline (excluding incomplete and potential host gene sequences) was checked using hierarchical clustering with the *h-cd-hit-est* program from the CD-HIT Suite Server (<http://weizhongli-lab.org/cd-hit/>)⁷². The 580 initial sequences were grouped (reverse compliments considered) using iterative cutoffs of 90%, 85% and 80% sequence identity to form 347 clusters. Custom scripts were then used to identify the number of different taxa present in each cluster based on sequence definitions. Representative sequences for each cluster were then blasted against the NCBI nucleotide (nt) database using Blast2GO⁶⁴ for annotation.

Repeat-induced point mutation identification. TE families for each genome were searched for signatures of RIP activity using the RIPCAL vr. 2 program^{73,74}. The program was only used to check for RIP within individual TE families which contained a minimum of ten sequences, with one or more sequence ≥ 300 bp (the default RIPCAL scanning subsequence length), using both the alignment with ClustalW⁷⁵ and di-nucleotide frequency-based methods. These cutoff criteria were established to minimize computational requirements, as several of the genome assemblies were relatively fragmented. RIP was considered present if di-nucleotide frequencies matched the indices: $(TpA/ApT) \geq 0.89$ and $(CpA + TpG)/(ApC + GpT) \leq 1.03$ ⁷⁶ and visual inspection of RIPCAL alignments showed one or more peaks for $(CA \leftarrow \rightarrow TA) + (TG \leftarrow \rightarrow TA)$ mutations⁷³. Additional details about the RIPCAL program can be found in Hane and Oliver⁷³.

References

- Dean, R. *et al.* The Top 10 fungal pathogens in molecular plant pathology. *Mol Plant Pathol* **13**, 414–430 (2012).
- Khush, G. S. What it will take to feed 5.0 billion rice consumers in 2030. *Plant Mol Biol* **59**, 1–6 (2005).
- Wilson, R. A. & Talbot, N. J. Under pressure: investigating the biology of plant infection by *Magnaporthe oryzae*. *Nat Rev Microbiol* **7**, 185–195 (2009).
- Urashima, A. S., Igarashi, S. & Kato, H. Host range, mating type, and fertility of *Pyricularia grisea* from wheat in Brazil. *Plant Dis* **77**, 1211–1216 (1993).
- Urashima, A. S. & Silva, C. P. Characterization of *Magnaporthe grisea* (*Pyricularia grisea*) from Black Oat in Brazil. *J Phytopathol* **159**, 789–795 (2011).
- Dean, R. A. *et al.* The genome sequence of the rice blast fungus *Magnaporthe grisea*. *Nature* **434**, 980–986 (2005).
- Xu, J. R., Zhao, X. H. & Dean, R. A. From genes to genomes: a new paradigm for studying fungal pathogenesis in *Magnaporthe oryzae*. *Fungal Genomics* **57**, 175–218 (2007).
- Okagaki, L. H. *et al.* Genome sequences of three phytopathogenic species of the Magnaporthaceae family of fungi. *G3-Genes Genom Genet* **5**, 2539–2545, <https://doi.org/10.1534/g3.115.020057> (2015).
- Luo, J. *et al.* Phylogenomic analysis uncovers the evolutionary history of nutrition and infection mode in rice blast fungus and other Magnaporthales. *Scientific Reports* **5**, 9448 (2015).
- Stamatakis, A. RAxML-VI-HPC: maximum likelihood-based phylogenetic analyses with thousands of taxa and mixed models. *Bioinformatics* **22**, 2688–2690 (2006).
- Doolittle, R. F., Feng, D. F., Tsang, S., Cho, G. & Little, E. Determining divergence times of the major kingdoms of living organisms with a protein clock. *Science* **271**, 470–477, <https://doi.org/10.1126/Science.271.5248.470> (1996).
- Heckman, D. S. *et al.* Molecular evidence for the early colonization of land by fungi and plants. *Science* **293**, 1129–1133, <https://doi.org/10.1126/Science.1061457> (2001).
- Taylor, T. N., Hass, T. & Kerp, H. The oldest fossil ascomycetes. *Nature* **399**, 648–648, <https://doi.org/10.1038/21349> (1999).
- Rieux, A. & Balloux, F. Inferences from tip-calibrated phylogenies: a review and a practical guide. *Mol Ecol* **25**, 1911–1924, <https://doi.org/10.1111/mec.13586> (2016).
- Lynch, M. Evolution of the mutation rate. *Trends Genet* **26**, 345–352, <https://doi.org/10.1016/j.tig.2010.05.003> (2010).
- Gladyshev, E. A., Meselson, M. & Arkhipova, I. R. Massive horizontal gene transfer in bdelloid rotifers. *Science* **320**, 1210–1213, <https://doi.org/10.1126/science.1156407> (2008).
- Alexander, W. G., Wisecaver, J. H., Rokas, A. & Hittinger, C. T. Horizontally acquired genes in early-diverging pathogenic fungi enable the use of host nucleosides and nucleotides. *P Natl Acad Sci USA* **113**, 4116–4121, <https://doi.org/10.1073/pnas.1517242113> (2016).
- Marcet-Houben, M. & Gabaldon, T. Acquisition of prokaryotic genes by fungal genomes. *Trends Genet* **26**, 5–8, <https://doi.org/10.1016/j.tig.2009.11.007> (2010).
- Qiu, H., Cai, G. H., Luo, J., Bhattacharya, D. & Zhang, N. Extensive horizontal gene transfers between plant pathogenic fungi. *Bmc Biol* **14**, <https://doi.org/10.1186/S12915-016-0264-3> (2016).
- Thiyagarajan, S., Zhou, Z., Munteanu, L., Chang, F. & O’Shaughnessy, B. The Actomyosin Contractile Ring Regulates Septation during Fission Yeast Cytokinesis. *Biophys J* **106**, 358A–358A (2014).
- Pringle, J. R., Broach, J. R. & Jones, E. W. *The Molecular and Cellular Biology of the Yeast Saccharomyces; Cell Cycle and Cell Biology (Monograph 21c) 1st Ed.*, (NY: Cold Spring Harbor Laboratory Press, 1997).
- Bartek, J., Lukas, C. & Lukas, J. Checking on DNA damage in S phase. *Nat Rev Mol Cell Bio* **5**, 792–804, <https://doi.org/10.1038/nrm1493> (2004).
- Weiberg, A. *et al.* Fungal small RNAs suppress plant immunity by hijacking host RNA interference pathways. *Science* **342**, 118–123, <https://doi.org/10.1126/science.1239705> (2013).
- Furuya, K. & Niki, H. The DNA damage checkpoint regulates a transition between yeast and hyphal growth in *Schizosaccharomyces japonicus*. *Mol Cell Biol* **30**, 2909–2917, <https://doi.org/10.1128/MCB.00049-10> (2010).
- Park, C. H. *et al.* The *Magnaporthe oryzae* effector AvrPiz-t targets the RING E3 ubiquitin ligase API6 to suppress pathogen-associated molecular pattern-triggered immunity in rice. *Plant Cell* **24**, 4748–4762, <https://doi.org/10.1105/tpc.112.105429> (2012).
- Lo Presti, L. *et al.* Fungal effectors and plant susceptibility. *Annu Rev Plant Biol* **66**, 513–545, <https://doi.org/10.1146/annurev-arplant-043014-114623> (2015).
- Mentlak, T. A. *et al.* Effector-mediated suppression of chitin-triggered immunity by *Magnaporthe oryzae* Is necessary for rice blast disease. *Plant Cell* **24**, 322–335, <https://doi.org/10.1105/tpc.111.092957> (2012).

28. Sharpee, W. *et al.* Identification and characterization of suppressors of plant cell death (SPD) effectors from *Magnaporthe oryzae*. *Mol Plant Pathol* **18**, 850–863, <https://doi.org/10.1111/mpp.12449> (2017).
29. Saitoh, H. *et al.* Large-Scale Gene Disruption in *Magnaporthe oryzae* Identifies MC69, a Secreted Protein Required for Infection by Monocot and Dicot Fungal Pathogens. *Plos Pathog* **8**, <https://doi.org/10.1371/journal.ppat.1002711> (2012).
30. Mosquera, G., Giraldo, M. C., Khang, C. H., Coughlan, S. & Valent, B. Interaction transcriptome analysis identifies *Magnaporthe oryzae* BAS1-4 as biotrophy-associated secreted proteins in rice blast disease. *Plant Cell* **21**, 1273–1290, <https://doi.org/10.1105/tpc.107.055228> (2009).
31. Gao, X. & Lynch, M. Ubiquitous internal gene duplication and intron creation in eukaryotes. *P Natl Acad Sci USA* **106**, 20818–20823, <https://doi.org/10.1073/pnas.0911093106> (2009).
32. Xu, X. H. *et al.* The rice endophyte *Harpophora oryzae* genome reveals evolution from a pathogen to a mutualistic endophyte. *Scientific Reports* **4**, <https://doi.org/10.1038/Srep05783> (2014).
33. Flutre, T., Duprat, E., Feuillet, C. & Quesneville, H. Considering transposable element diversification in *de novo* annotation approaches. *Plos One* **6**, <https://doi.org/10.1371/journal.pone.0016526> (2011).
34. Thon, M. R., Martin, S. L., Goff, S., Wing, R. A. & Dean, R. A. BAC end sequences and a physical map reveal transposable element content and clustering patterns in the genome of *Magnaporthe grisea*. *Fungal Genet Biol* **41**, 657–666, <https://doi.org/10.1016/j.fgb.2004.02.003> (2004).
35. Couch, B. C. *et al.* Origins of host-specific populations of the blast pathogen *Magnaporthe oryzae* in crop domestication with subsequent expansion of pandemic clones on rice and weeds of rice. *Genetics* **170**, 613–630, <https://doi.org/10.1534/genetics.105.041780> (2005).
36. Ebbole, D. J. *Magnaporthe* as a model for understanding host-pathogen interactions. *Annual Review of Phytopathology* **45**, 437–456, <https://doi.org/10.1146/annurev.phyto.45.062806.094346> (2007).
37. Tucker, S. L. *et al.* Common genetic pathways regulate organ-specific infection-related development in the rice blast fungus. *Plant Cell* **22**, 953–972, <https://doi.org/10.1105/tpc.109.066340> (2010).
38. Bolger, A. M., Lohse, M. & Usadel, B. Trimmomatic: a flexible trimmer for Illumina sequence data. *Bioinformatics* **30**, 2114–2120, <https://doi.org/10.1093/bioinformatics/btu170> (2014).
39. Luo, R. *et al.* SOAPdenovo2: an empirically improved memory-efficient short-read *de novo* assembler. *GigaScience* **1**, 1–6, <https://doi.org/10.1186/2047-217X-1-18> (2012).
40. Parra, G., Bradnam, K. & Korf, I. CEGMA: a pipeline to accurately annotate core genes in eukaryotic genomes. *Bioinformatics* **23**, 1061–1067, <https://doi.org/10.1093/bioinformatics/btm071> (2007).
41. Parra, G., Bradnam, K., Ning, Z., Keane, T. & Korf, I. Assessing the gene space in draft genomes. *Nucleic Acids Res.* **37**, 289–297, <https://doi.org/10.1093/nar/gkn916> (2009).
42. Holt, C. & Yandell, M. MAKER2: an annotation pipeline and genome-database management tool for second-generation genome projects. *BMC Bioinformatics* **12**, 491–491, <https://doi.org/10.1186/1471-2105-12-491> (2011).
43. Stanke, M. & Waack, S. Gene prediction with a hidden Markov model and a new intron submodel. *Bioinformatics* **19**, ii215–ii225, <https://doi.org/10.1093/bioinformatics/btg1080> (2003).
44. Stanke, M., Schoffmann, O., Morgenstern, B. & Waack, S. Gene prediction in eukaryotes with a generalized hidden Markov model that uses hints from external sources. *BMC Bioinformatics* **7**, 62 (2006).
45. Korf, I. Gene finding in novel genomes. *BMC Bioinformatics* **5**, 59, <https://doi.org/10.1186/1471-2105-5-59> (2004).
46. Ter-Hovhannisyan, V., Lomsadze, A., Chernoff, Y. O. & Borodovsky, M. Gene prediction in novel fungal genomes using an ab initio algorithm with unsupervised training. *Genome Res.* **18**, 1979–1990, <https://doi.org/10.1101/gr.081612.108> (2008).
47. Grabherr, M. G. *et al.* Full-length transcriptome assembly from RNA-Seq data without a reference genome. *Nat Biotech* **29**, 644–652, <http://www.nature.com/nbt/journal/v29/n7/abs/nbt.1883.html#supplementary-information> (2011).
48. Bairoch, A. & Apweiler, R. The SWISS-PROT protein sequence database and its supplement TrEMBL in 2000. *Nucleic Acids Res.* **28**, 45–48 (2000).
49. Emms, D. M. & Kelly, S. OrthoFinder: solving fundamental biases in whole genome comparisons dramatically improves orthogroup inference accuracy. *Genome Biol* **16**, 157, <https://doi.org/10.1186/s13059-015-0721-2> (2015).
50. Ranwez, V., Harispe, S., Delsuc, F. & Douzery, E. J. P. MACSE: Multiple Alignment of Coding SEquences Accounting for Frameshifts and Stop Codons. *Plos One* **6**, <https://doi.org/10.1371/journal.pone.0022594> (2011).
51. Drummond, M. T. Nurture of the beast. *Sport Educ Soc* **11**, 424–426 (2006).
52. Drummond, A. J. & Rambaut, A. BEAST: Bayesian evolutionary analysis by sampling trees. *Bmc Evol Biol* **7**, <https://doi.org/10.1186/1471-2148-7-214> (2007).
53. Kasuga, T., White, T. J. & Taylor, J. W. Estimation of nucleotide substitution rates in eurotiomycete fungi. *Mol Biol Evol* **19**, 2318–2324 (2002).
54. Edgar, R. C. Search and clustering orders of magnitude faster than BLAST. *Bioinformatics* **26**, 2460–2461, <https://doi.org/10.1093/bioinformatics/btq461> (2010).
55. Wisecaver, J. H., Alexander, W. G., King, S. B., Hittinger, C. T. & Rokas, A. Dynamic evolution of nitric oxide detoxifying flavohemoglobins, a family of single-protein metabolic modules in bacteria and eukaryotes. *Mol Biol Evol* **33**, 1979–1987, <https://doi.org/10.1093/molbev/msw073> (2016).
56. Edgar, R. C. MUSCLE: a multiple sequence alignment method with reduced time and space complexity. *Bmc Bioinformatics* **5**, 113 (2004).
57. Capella-Gutierrez, S., Silla-Martinez, J. M. & Gabaldon, T. trimAl: a tool for automated alignment trimming in large-scale phylogenetic analyses. *Bioinformatics* **25**, 1972–1973, <https://doi.org/10.1093/bioinformatics/btp348> (2009).
58. Price, M. N., Dehal, P. S. & Arkin, A. P. FastTree 2-approximately maximum-likelihood trees for large alignments. *Plos One* **5**, <https://doi.org/10.1371/journal.pone.0009490> (2010).
59. Shimodaira, H. & Hasegawa, M. Multiple comparisons of log-likelihoods with applications to phylogenetic inference. *Mol Biol Evol* **16**, 1114–1116 (1999).
60. Katoh, K. & Standley, D. M. MAFFT multiple sequence alignment software version 7: improvements in performance and usability. *Mol Biol Evol* **30**, 772–780, <https://doi.org/10.1093/molbev/mst010> (2013).
61. Abascal, F., Zardoya, R. & Telford, M. J. TranslatorX: multiple alignment of nucleotide sequences guided by amino acid translations. *Nucleic Acids Res* **38**, W7–W13, <https://doi.org/10.1093/nar/gkq291> (2010).
62. Gouveia-Oliveira, R., Sackett, P. W. & Pedersen, A. G. MaxAlign: maximizing usable data in an alignment. *Bmc Bioinformatics* **8**, <https://doi.org/10.1186/1471-2105-8-312> (2007).
63. Yang, Z. PAML 4: phylogenetic analysis by maximum likelihood. *Mol Biol Evol* **24**, 1586–1591, <https://doi.org/10.1093/molbev/msm088> (2007).
64. Conesa, A. & Gotz, S. Blast2GO: A comprehensive suite for functional analysis in plant genomics. *Int J Plant Genomics* **619832**, (2008).
65. Enright, A. J., Van Dongen, S. & Ouzounis, C. A. An efficient algorithm for large-scale detection of protein families. *Nucleic Acids Res* **30**, 1575–1584, <https://doi.org/10.1093/Nar/30.7.1575> (2002).
66. Kim, K. T. *et al.* Kingdom-wide analysis of fungal small secreted proteins (SSPs) reveals their potential role in host association. *Front Plant Sci* **7**, <https://doi.org/10.3389/Fpfs.2016.00186> (2016).

67. Valent, B. & Khang, C. H. Recent advances in rice blast effector research. *Curr Opin Plant Biol* **13**, 434–441, <https://doi.org/10.1016/j.pbi.2010.04.012> (2010).
68. Camacho, C. *et al.* BLAST plus: architecture and applications. *Bmc Bioinformatics* **10**, <https://doi.org/10.1186/1471-2105-10-421> (2009).
69. Jurka, J. *et al.* Repbase update, a database of eukaryotic repetitive elements. *Cytogenet Genome Res* **110**, 462–467, <https://doi.org/10.1159/000084979> (2005).
70. Finn, R. D. *et al.* Pfam: the protein families database. *Nucleic Acids Res* **42**, D222–D230, <https://doi.org/10.1093/nar/gkt1223> (2014).
71. Wicker, T. *et al.* A unified classification system for eukaryotic transposable elements. *Nat Rev Genet* **8**, 973–982, <https://doi.org/10.1038/nrg2165> (2007).
72. Huang, Y., Niu, B. F., Gao, Y., Fu, L. M. & Li, W. Z. CD-HIT Suite: a web server for clustering and comparing biological sequences. *Bioinformatics* **26**, 680–682, <https://doi.org/10.1093/bioinformatics/btq003> (2010).
73. Hane, J. K. & Oliver, R. P. RIPCAL: a tool for alignment-based analysis of repeat-induced point mutations in fungal genomic sequences. *Bmc Bioinformatics* **9**, <https://doi.org/10.1186/1471-2105-9-478> (2008).
74. Hane, J. K. In *Genetic Transformation Systems in fungi* Vol. 2 69–78 (Springer International Publishing, 2015).
75. Larkin, M. A. *et al.* Clustal W and clustal X version 2.0. *Bioinformatics* **23**, 2947–2948, <https://doi.org/10.1093/bioinformatics/btm404> (2007).
76. Margolin, B. S. *et al.* A methylated *Neurospora* 5S rRNA pseudogene contains a transposable element inactivated by repeat-induced point mutation. *Genetics* **149**, 1787–1797 (1998).

Acknowledgements

This work is funded by the National Science Foundation (DEB 1145174) to NZ and DB, the Rutgers Center for Turfgrass Science, the Rutgers School of Environmental and Biological Sciences, and was the outcome of an international symposium hosted by NZ and DB at Rutgers University. We thank Ralph Dean, Nicole Donofrio, Mark Farman, Li-Jun Ma, Thomas Mitchell, Kerry Pedley, Youliang Peng, Barbara Robbertse, Antonis Rokas, Darren Soanes, Nicholas Talbot, Didier Tharreau, Michael Thon, Barbara Valent, and Jin-Rong Xu for participating the symposium and/or discussion.

Author Contributions

N.Z. and D.B. designed the study and were in charge of manuscript preparation and revision. G.C. did the fungal genome assembly and annotation, D.C.P. did the test for positive selection, H.Q. and J.H.W. did the H.G.T. analyses, Y.H.L., J.Z. and C.H.K. did the secretome analysis, P.G. did the diversification timing analysis, J.A.C. and D.V. did the transposon analysis. All authors participated in manuscript writing and revision.

Additional Information

Supplementary information accompanies this paper at <https://doi.org/10.1038/s41598-018-24301-6>.

Competing Interests: The authors declare no competing interests.

Publisher's note: Springer Nature remains neutral with regard to jurisdictional claims in published maps and institutional affiliations.



Open Access This article is licensed under a Creative Commons Attribution 4.0 International License, which permits use, sharing, adaptation, distribution and reproduction in any medium or format, as long as you give appropriate credit to the original author(s) and the source, provide a link to the Creative Commons license, and indicate if changes were made. The images or other third party material in this article are included in the article's Creative Commons license, unless indicated otherwise in a credit line to the material. If material is not included in the article's Creative Commons license and your intended use is not permitted by statutory regulation or exceeds the permitted use, you will need to obtain permission directly from the copyright holder. To view a copy of this license, visit <http://creativecommons.org/licenses/by/4.0/>.

© The Author(s) 2018